

ZAMM



<https://onlinelibrary.wiley.com/journal/15214001>

Accepted January 7th, 2024.

MATHEMATICAL MODELLING OF COUPLE STRESS FLUID FLOW AROUND A SEMI-PERMEABLE SPHERE ENCLOSING A SOLID CORE

R. Selvi*

Institute of Mathematical Sciences, Chennai-600113, India.

*Corresponding author - Email: selvir@imsc.res.in

O. Anwar Bég

Professor and Director- Multi-Physical Engineering Sciences Group, Aeronautical and Mechanical Engineering Department, Corrosion and Coating Lab, SEE Building, Room 3-08, Salford University, Manchester, M54WT, UK.

Email: O.A.Beg@salford.ac.uk

ABSTRACT: The focus of this article is to study theoretically the steady-axisymmetric creeping flow dynamics of a couple stress fluid external to a semi-permeable sphere containing a solid core. This problem is motivated by emulsion hydrodynamics in chemical engineering where rheological behaviour often arises in addition to porous media effects. The non-Newtonian Stokes' couple stress fluid model features couple stresses and body couples that are absent in the classical Navier-Stokes viscous model. It provides a robust framework for simulating emulsions, complex suspensions and other liquids which possess microstructure. The physical regime is delineated into two zones- the interior of the semi-permeable zone (region II) which engulfs the solid core and the external couple stress fluid zone (region I). The model is formulated using a spherical polar coordinate system in terms of the stream function ψ . The Brinkman-extended Darcy model is deployed for the porous medium hydrodynamics and isotropic permeability is considered. Analytical expressions are derived for dimensionless pressure, tangential stress and the couple stress components using the method of separation of variables and Gegenbauer functions of the first kind. The integration constants are evaluated with appropriate boundary conditions on the inner and outer boundary of the semi-permeable zone with the aid of Mathematica symbolic software. Solutions for the drag force exerted by the couple stress fluid on the semi-permeable sphere and volumetric flow rate are also derived with corresponding expressions for the drag coefficient and non-dimensional volumetric flow rate. The influence of permeability (k), separation parameter (l), couple stress viscosity coefficient (η), couple stress inverse length dependent parameter ($\lambda = \sqrt{\mu/\eta}$) and couple stress viscosity ratio ($\tau = \eta/\eta'$) on all key variables is studied graphically. Additionally streamline contours are computed for a range of parameters including inverse permeability parameter ($\alpha = 1/k$). The computations show that increasing couple stress inverse length dependent parameter (λ) greatly reduces the dimensionless volumetric flow rate in particular at high values of separation parameter (l). Flow rate is however markedly enhanced with permeability (k) and also couple stress viscosity parameter (η). In the presence of the solid core a much greater drag coefficient is observed at all values of couple stress inverse length dependent parameter (λ) relative to the case without a solid core. A significant distortion in streamlines is computed with increasing separation parameter (l) with a dual vortex structure emanating. With greater couple stress viscosity parameter (τ) no tangible modification is observed in the streamline contours. The present work generalizes the earlier study of Krishnan and Shukla (2021) to consider a semi-permeable (porous medium) outer sphere and furthermore presents detailed streamline visualizations of the creeping flow for a range of emerging parameters of relevance to non-Newtonian chemical engineering processes including emulsion droplet dynamics in porous materials.

KEYWORDS: Couple stress non-Newtonian fluid; viscosity ratio, radius ratio, permeability; flow rate; streamline visualization; Drag coefficient; chemical engineering.

NOMENCLATURE

Roman

a	<i>radius of solid core</i>
A_1	<i>Integration constant</i>
A_2	<i>Integration constant</i>
b	<i>radius to outer wall of outer semi-permeable sphere (region II)</i>
B_1	<i>Integration constant</i>
B_2	<i>Integration constant</i>
$\overline{dij}^{(i)}$	<i>Deformation rate tensor</i>
D_N	<i>Non-dimensional drag coefficient</i>
E^2	<i>Stokes' operator</i>
F	<i>Drag force</i>
$G_2(\zeta)$	<i>Gegenbauer functions of the first kind</i>
k	<i>Permeability of saturated porous medium sphere encasing solid core sphere</i>
l	<i>separation parameter (a/b)</i>
$m_{r\phi}$	<i>Couple stress component</i>
Q	<i>Volumetric flow rate</i>
Q_N	<i>Non-dimensional flow rate</i>
p	<i>Fluid pressure</i>
r	<i>radial coordinate</i>
u_r, u_θ	<i>Radial and tangential velocity components</i>

Greek

α	<i>inverse permeability parameter (=1/k)</i>
λ	<i>Couple stress inverse length dependent parameter</i>
η, η'	<i>Couple stress viscosity coefficients</i>
ψ	<i>Dimensional stream function</i>
μ_1	<i>Dynamic viscosity of fluid in semi-permeable sphere</i>
μ_2	<i>Dynamic viscosity of couple stress region (external to sphere)</i>
θ	<i>polar coordinate</i>
ϕ	<i>azimuthal coordinate</i>
τ	<i>Couple stress viscosity ratio (= η/η')</i>
$\tau_{r\theta}$	<i>Shear stress component</i>

1.INTRODUCTION

The couple stress fluid theory was introduced by Stokes [1] by incorporating couple stresses and body couples in the classical Navier-Stokes viscous flow model. The concept of couple stresses arise due to the way in which the mechanical interactions in the fluid medium are modelled. These non-Newtonian fluids are also termed “polar” fluids [2]. Couple stress theory provides an elegant framework for simulating the rheology of complex industrial and biological fluids. The stress tensors for couple stress fluids are not symmetric and can capture length effect which is not possible with the classical Navier-Stokes model. However, they are simpler than micropolar fluids [3] since they possess no microstructure at the kinematic level and therefore the kinematics of such fluids is totally described using the velocity field. As such a

supplementary angular momentum (micro-rotation vector) equation is not required for couple stress fluids. The couple stress effects are all encapsulated in the modified linear momentum equations (Navier-Stokes). The mechanical interactions in the fluid medium that penetrate the surface create couple stresses. The relative simplicity of couple stress fluids have made them very attractive for simulating a wide spectrum of problems in engineering where suspended particle effects can be simulated with the additional couple stress terms. These applications have included biomedical and chemical engineering science processes. Relevant works include Naduvinamani and Patil [4], Walicki and Walicka [5] and Lin and Huang [6] all addressing couple stress effects in lubrication flows. Biophysical studies have included Bég *et al.* [7] (on centrifugal blood flow separation) and Ali *et al.* [8] (on embryological propulsion). Chemical materials processing studies include Ramana Murthy *et al.* [9] (on thermo-rheological duct processing) and Nagaraju *et al.* [10] (on stretching sheet coating dynamics). Further investigations have considered couple stress working fluids in bio-inspired electromagnetic pumping [11]. All these studies have confirmed the considerable modification in transport characteristics induced by couple stresses relative to Newtonian formulations.

Another important category of non-Newtonian flows involves the creeping dynamics from a spherical geometry. This framework can be utilized to simulate droplet hydrodynamics, emulsions and many other areas of chemical engineering transport phenomena. Many different rheological models have been deployed in assessing such flows including viscoelastic, power-law, Stokes couple stress [12] and Eringen micropolar [13] models, all of which capture different non-Newtonian characteristics. The slow steady flow of couple stress fluids external to axisymmetric bodies has been studied by Ramkissoon [14] who derived an expression for drag experienced by a sphere using a stream function approach and also presented comparisons with the micropolar model. Devakar and Iyengar [15] derived analytical solutions for Stokes' first and second oscillatory plate problem using Laplace transforms. Devakar and Iyengar [16] further computed the run up flow between parallel plates for an incompressible couple stress fluid. Iyengar and Vani [17] considered the creeping flow of couple stress fluids between two confocal oblate spheroidal bodies slowly rotating about a common axis of symmetry with different angular speeds. They used Legendre functions, oblate spheroidal radial and angular wave functions to derive expressions for velocity and the couple experienced by the spheroids and noted that enhancement in couple stress is caused by increasing the rate of rotation of the spheroids. Devakar *et al.* [18] studied the effects of slip boundary conditions in Couette and Poiseuille flows of a couple stress fluid. Ashmawy [19] investigated the drag on a rigid slowly moving sphere engulfed with couple stress fluid showing that greater drag is present with

couple stresses present compared with the Newtonian viscous case (negligible length dependence effects). Vani and Ravi Kant [20] considered the oscillatory flow of an incompressible couple stress fluid between two slowly spinning and vibrating concentric spheres with equal oscillation frequency but dissimilar rotational velocities. Ramalakshmi and Shukla [21] conducted a rigorous analysis of the creeping flow of couple stress fluid from a sphere containing a solid core. They computed the drag coefficient analytically and showed that as couple stress parameter (inverse length dependence) increases the velocity, drag force and the pressure decreases. However, they also noted that with increasing couple stress viscosity coefficient is elevated the drag is also increased. Furthermore, they found that with greater couple stress parameter and radius ratio (i. e. the normalized distance from the surface of the sphere) there is a decrement in pressure.

The above studies neglected the inclusion of porous (permeable) media. They considered only purely fluent media. However, in many chemical and biomedical flow applications, a porous medium may be present. These include packed beds, filtration materials, biological tissue, droplets in foams etc. The classical approach for simulating fluid percolation in a porous medium was developed by the French engineer, Darcy [22]. The famous law named after him assumes that the flow is proportional to the drop in pressure across the porous medium and features the permeability i. e. hydraulic conductivity. For densely packed porous media the permeability is low and vice versa for sparsely packed materials. Both situations can arise in chemical engineering. Indeed, packed beds may exhibit a range of permeabilities depending on the application under consideration. Darcy's model is restricted to viscous-dominated transport where inertial effects are neglected. However, it is not founded on the basis of the Navier-Stokes equations framework. Furthermore, it cannot accommodate materials with very high porosity values. The Dutch petroleum engineer, Brinkman [23] modified the Darcy formulation by considering the transport of a spherical particle in a porous medium and derived a relationship between permeability and particle size and density, also corroborating his results with the empirical Carman model [24]. This formulation which considers the Stokes equations (neglecting inertial terms) has come to be known as the Darcy-Brinkman model and is one of the best approaches available for simulating creeping viscous flows in porous media. It also features an effective viscosity. Joseph and Tao [25] applied the Darcy-Brinkman model to study the streaming flow of an incompressible viscous fluid past a permeable spherical particle. They showed that the drag on the permeable sphere is equivalent to the drag on a solid (impermeable) sphere with the radius reduced. The Darcy-Brinkman model however has limitations and cannot accommodate very high porosity and high shear rates (inertial effects).

Several other investigators have addressed the problem of drag effects on a spherical particle in a porous medium including Tam [26] who showed that the drag in low Reynolds number flow is a function of the first three moments of the particle size distribution. Ludgren [27] re-examined the drag effect on porous media bed transport by generalizing Brinkman's model to both stationary beds and suspensions using the Stokes equations (inertia negligible). His solution for stationary beds concurred with Brinkman's model for permeability. Subsequently many investigators have adopted the Darcy-Brinkman model (and its modifications) to examine a range of non-Newtonian flows. Raptis and Takhar [28] studied the boundary layer flow of a couple stress fluid from an infinite wall using the Darcy-Brinkman-Forchheimer porous medium, to include inertial drag effects. They computed the velocity evolution for a range of permeability parameters. Hiremath and Patil [29] derived perturbation solutions for couple stress (polar) fluid thermal convective flow from an oscillating wall to a porous medium. They showed that couple stresses induce significant cooling in the regime and lower velocities compared with Newtonian liquids and that increasing permeability and thermal buoyancy force respectively accelerate and decelerate the flow. Umavathi and Bég [30] investigated numerically the thermo-convective stability of a couple-stress nanofluid saturated permeable layer using a Galerkin weighted residual method. They conducted both linear and non-linear stability analysis and showed that increasing couple-stress parameter (ratio of couple stress viscosity to dynamic viscosity) exerts a stabilizing effect on both the stationary and oscillatory convection modes. They also showed that increasing Vadász number (an inverse function of Darcy permeability parameter) tends to destabilize the oscillatory convection mode. Creeping Stokesian flows both inside permeable bodies and external to permeable layers have also been addressed with the Darcy-Brinkman approach for a range of microstructural liquids. Srinivasacharya D and Rajyalakshmi [31] determined the drag force in creeping flow of a micropolar incompressible fluid external to a porous sphere with permeability effects. They found that the resistance force decreases as the Eringen coupling number (ratio of vortex viscosity to dynamic viscosity) decreases whereas it is elevated as the permeability parameter decreases. Gupta and Deo [32] derived analytical solutions for Stokes flow of a micropolar fluid through a permeable sphere. They used non-homogenous boundary conditions for the microrotation vector and obtained an expression for the drag exerted by the sphere. They observed that there is a decrement in drag force with increasing Eringen coupling number and decreasing permeability of the porous medium. Aparna *et al.* [33, 34] computed the oscillatory and uniform steady flows, respectively of a couple stress fluid through a permeable sphere using the Darcy-Brinkman model. Radhika and Iyengar [35] investigated the Stokes flow of a

couple stress fluid external to a pair of confocal prolate spheroids, with the inner most shell contains couple stress fluid, surrounded by a porous medium (annular region). They noted that permeability and couple stress parameter strongly modify velocity and drag force and that with increment in eccentricity of the outer spheroid there is an elevation in the drag. Selvi and Shukla [36] studied the Stokesian dynamics from a porous medium sphere containing viscous Newtonian fluid surrounded by micropolar fluid external to the sphere. They determined the stream functions via matching the solution of the Brinkman equation with the Stokes equation. They computed the effects of permeability on drag force and drag coefficient numerically. Numerous other studies of this type have been reported for different combinations of the fluid saturating the porous medium and the encasing fluid. These include Selvi *et al.* [37] who studied the case of a viscoelastic fluid in the porous inner shell engulfed in a micropolar fluid). Selvi *et al.* [38] considered a three-zone model with an inner core of Reiner–Rivlin non-Newtonian liquid particle, surrounded with a Newtonian liquid shell and encased in a permeable medium. Selvi and Shukla [39] addressed the two-zone case of a Reiner-Rivlin liquid sphere surrounded by a micropolar fluid with Mehta-Morse boundary conditions and asymptotic expansions. El-Sapa and Alsudais [40] considered the hydromagnetic slip flow of Newtonian concentric spheres surrounded with a porous medium. Namdeo and Gupta [41] considered the electrically conducting flow over a sphere inside a semipermeable shell in the presence of the magnetic field using a Darcy model, noting that increasing magnetic field enhances the drag on the composite sphere, and that an impermeable sphere experiences greater drag than a permeable sphere. Madasu and Sarkar [42] simulated the case of a couple stress fluid streaming past a solid spherical body in a permeable Brinkman medium with wall slip effects. They showed that as the slip parameter increases, drag increases and surface velocity on the sphere is depleted. Sakthivel and Pankaj [43] studied the Stokes flow through a couple stress fluid enclosed by a permeable medium. They showed that lower drag is produced for couple stress fluids compared with Newtonian fluids.

A scrutiny of the literature has identified that steady-axisymmetric creeping Stokesian flow of a couple stress fluid external to a semi-permeable sphere saturated with couple stress fluid and containing a solid core, has thus far not been addressed with the Darcy-Brinkman formulation. This is the focus and novelty of the current investigation. In the present article analytical solutions are derived for this problem. Expressions are presented for velocity, pressure, shear stress, couple stress, drag force and volumetric flow rate with the aid of orthogonal polynomials. The dimensionless drag coefficient and non-dimensional volumetric flow rate are also obtained. Numerical evaluations of the solutions are executed in MATHEMATICA

software. A parametric study of the influence of permeability (k), separation parameter (l), couple stress viscosity coefficient (η), couple stress inverse length dependent parameter ($\lambda = \sqrt{\mu/\eta}$) and couple stress viscosity ratio ($\tau = (\eta/\eta')$) on all key variables is conducted. Extensive visualization is included additionally for streamline contours. Special cases of the general model are extracted to compare with earlier published works. Extensive physical interpretation of the graphical results is included. The present work generalizes the earlier study of Krishnan and Shukla [21] who ignored permeability effects, to consider a permeable outer sphere and furthermore presents detailed streamline visualizations of the creeping flow for a range of emerging parameters of relevance to non-Newtonian chemical engineering processes including oil or emulsion droplet motion in porous regimes [44] or lymph droplet intrusion into biological tissue [45].

2. MATHEMATICAL FORMULATION AND GEOMETRIC MODEL

The physical model under investigation is depicted in **Fig. 1**. The steady, axisymmetric flow of an incompressible couple stress (polar) fluid of viscosity η past a semipermeable sphere containing a solid sphere core is considered.

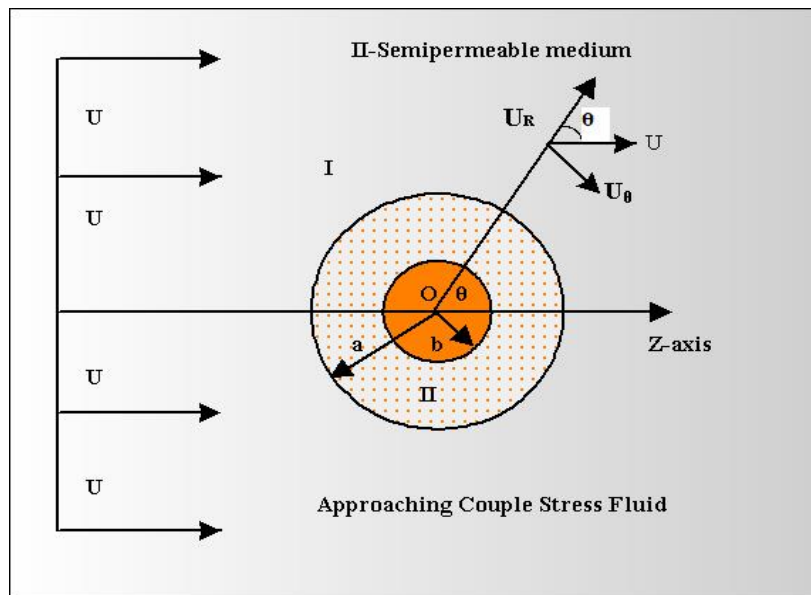


Fig. 1: Physical representation of regime

A spherical polar coordinate system (r, θ, ϕ) is adopted. The semipermeable medium is assumed to be isotropic and homogeneous and saturated with couple stress fluid. The characteristic (uniform) velocity U acts along the Z -direction of the fluid flow. O denotes the centre of the concentric spheres. The interior of the semipermeable layer is considered as

region II and the exterior of the couple stress fluid is consider as **region I**. The mass and momentum conservation equations for a polar (couple stress) fluid in vector form, following Stokes [46] is:

$$\operatorname{div} \vec{u}^{(1)} = 0, \quad (1)$$

$$\mu_1 \nabla^2 \vec{u}^{(1)} - \eta \nabla^4 \vec{u}^{(1)} = \nabla p^{(1)}. \quad (2)$$

Here $\vec{u}^{(1)}$ =velocity vector, η denotes coefficient of couple stress viscosity and μ_1 is the dynamic viscosity parameter. Mathematically, the motion of a couple stress fluid is therefore governed by an equation similar to the classical Navier–Stokes equation but with higher order. The internal governing equations for a semipermeable region are based on the Brinkman-extension to the Darcy law:

$$\operatorname{div} \vec{u}^{(2)} = 0, \quad (3)$$

$$- \frac{k}{\mu_2} \nabla p^{(2)} = \vec{u}^{(2)}. \quad (4)$$

Here μ_2 = dynamic viscosity of semi-permeable region fluid, $p^{(2)}$ is a pressure, k = permeability of the porous material which is assumed isotropic. A dimensional stream function, ψ is introduced (to define the velocity components in the radial and polar directions) which satisfies the continuity equation $\operatorname{div} \vec{u} = 0$ by virtue of the Cauchy-Riemann equations in spherical polar coordinates:

$$u_r = -\frac{1}{r^2 \sin \theta} \frac{\partial \psi}{\partial \theta}, \quad u_\theta = -\frac{1}{r \sin \theta} \frac{\partial \psi}{\partial r}, \quad (5)$$

Using equation (5), we eliminate the pressure term from equations (2) and (4) which yields:

$$E^4(E^2 - \lambda^2)\psi^{(1)} = 0, \quad (6)$$

$$E^2\psi^{(2)} = 0. \quad (7)$$

Here the Stokes' operator E^2 is given by $E^2 = \frac{\partial}{\partial r^2} + \frac{\sin \theta}{r^2} \frac{\partial}{\partial \theta} \left(\frac{1}{\sin \theta} \frac{\partial}{\partial \theta} \right)$. Also $\lambda^2 = \frac{\mu}{\eta}$ is the couple stress parameter i. e. ratio of dynamic (Newtonian) viscosity to couple stress viscosity coefficient.

Using Eqns. (6) and (7), the stream function can be determined by implementing the method of separation of variables as follows:

$$\psi^{(1)}(r, \zeta) = \left[r^2 + A_1 r + A_2 r^{-1} + A_3 \left(1 + \frac{1}{\lambda r} \right) e^{-\lambda r} \right] G_2(\zeta), \quad (8)$$

$$\psi^{(2)}(r, \zeta) = [B_1 r^2 + B_2 r^{-1}] G_2(\zeta). \quad (9)$$

Here $G_2(\zeta) = \frac{1}{2}(1 - \zeta^2)$ is a Gegenbauer function of the first kind and $\zeta = \cos\theta$. Important physical quantities are the pressure components, tangential stress and the couple stress which emerge as:

$$p^{(1)} = -\frac{2\mu_1 A_1}{r^2} \cos\theta, \quad (10)$$

$$p^{(2)} = \alpha^2 \left[B_1 r - \frac{B_2}{r^2} \right] \cos\theta, \quad (11)$$

$$\tau_{r\theta} = \mu \left[\frac{3A_2}{r^4} + A_3 \left(\frac{\lambda}{r^2} + \frac{3}{r^3} + \frac{3}{\lambda r^4} \right) e^{-\lambda r} \right] \sin\theta, \quad (12)$$

$$m_{r\phi} = \left[(2\eta + \eta') \left(\frac{2A_1}{r^3} - \lambda^2 A_3 \left[\frac{1}{r^2} + \frac{1}{\lambda r^3} \right] e^{-\lambda r} \right) - \eta \frac{\lambda^3}{r} A_3 e^{-\lambda r} \right] \sin\theta. \quad (13)$$

The expression for couple stress $m_{r\phi}$ is based on Stokes [47].

In Eqn. (11), the parameter, $\alpha = 1/k$. The coefficients A_1, A_2, A_3, B_1, B_2 are constants which can be determined with the help of boundary conditions described in due course.

3. BOUNDARY CONDITIONS

In order to evaluate the expressions (8)-(13) to quantify the hydrodynamic behaviour as influenced by mechanical properties of particles interactions, it is necessary to choose four appropriate boundary conditions on the inner and outer surfaces of the sphere. In this regard, the continuity of normal velocity, vanishing of tangential velocity, continuity of pressure, and vanishing of couple stress component $m_{r\theta}$ at ($r=1$) are considered. It follows that:

On the outer region at $r = I$:

$$\frac{\partial \psi^{(1)}}{\partial \theta} = \frac{\partial \psi^{(2)}}{\partial \theta}, \quad (14)$$

$$\frac{\partial \psi^{(1)}}{\partial r} = 0, \quad (15)$$

$$p^{(1)} = p^{(2)}, \quad (16)$$

$$m_{r\varphi} = 0. \quad (17)$$

On the inner region at $r = l$ ($l=b/a$ i. e. ratio of inner solid sphere core radius to semi-permeable sphere radius):

$$\frac{\partial \psi^{(2)}}{\partial \theta} = 0, \quad (18)$$

Introducing the boundary conditions from (14) to (18) into the expressions (8), (9), (10), (11) and (13), the following linear equations emerge:

$$A_1 + A_2 + A_3 \left(1 + \frac{1}{\lambda}\right) e^{-\lambda} = -1, \quad (19)$$

$$A_1 - A_2 - A_3 \left(1 + \lambda + \frac{1}{\lambda}\right) e^{-\lambda} = -2, \quad (20)$$

$$-2\mu_1 A_1 - \alpha^2 B_1 \mu_2 + \alpha^2 \frac{B_2}{2} \mu_2 = 0, \quad (21)$$

$$2(2 + \tau)A_1 + A_3 \left[-(2 + \tau)\lambda^2 \left(1 + \frac{1}{\lambda}\right) e^{-\lambda} - \lambda^3 e^{-\lambda}\right] = 0, \quad (22)$$

$$l^2 B_1 + \frac{B_2}{l} = 0. \quad (23)$$

Here τ designates the couple stress viscosity ratio ($=\eta/\eta'$). Solving the system of linear Eqns. (19) to (23), with Mathematica symbolic software, all the integration constants, A_1, A_2, A_3, B_1 and B_2 are determined as follows:

$$A_1 = \frac{3\alpha^2(l^3+2)(\lambda^2+\lambda(2+\tau)+2+\tau)}{2\left((2\alpha^2+1)\lambda^2+(2\alpha^2+1)\lambda(2+\tau)+l^3\left((\alpha^2-1)\lambda^2+(\alpha^2-1)\lambda(2+\tau)-2-\tau\right)+2+\tau\right)}, \quad (24)$$

$$A_2 = 2 - \frac{3\alpha^2(l^3+2)\left(\lambda^4+\lambda^3(2+\tau)-\lambda^2(2+\tau)-2\lambda(2+\tau)-2(2+\tau)\right)}{2\lambda^2\left((2\alpha^2+1)\lambda^2+(2\alpha^2+1)\lambda(2+\tau)+l^3\left((\alpha^2-1)\lambda^2+(\alpha^2-1)\lambda(2+\tau)-2-\tau\right)+2+\tau\right)}, \quad (25)$$

$$A_3 = -\frac{3\alpha^2(l^3+2)(2+\tau)e^\lambda}{\lambda\left((2\alpha^2+1)\lambda^2+(2\alpha^2+1)\lambda(2+\tau)+l^3\left((\alpha^2-1)\lambda^2+(\alpha^2-1)\lambda(2+\tau)-2-\tau\right)+2+\tau\right)}, \quad (26)$$

$$B_1 = -\frac{3(\lambda^2+\lambda(2+\tau)+2+\tau)}{(2\alpha^2+1)\lambda^2+(2\alpha^2+1)\lambda(2+\tau)+l^3\left((\alpha^2-1)\lambda^2+(\alpha^2-1)\lambda(2+\tau)-2-\tau\right)+2+\tau}, \quad (27)$$

$$B_2 = -\frac{3l^3(\lambda^2+\lambda(2+\tau)+2+\tau)}{(2\alpha^2+1)\lambda^2+(2\alpha^2+1)\lambda(2+\tau)+l^3((\alpha^2-1)\lambda^2+(\alpha^2-1)\lambda(2+\tau)-2-\tau)+2+\tau}. \quad (28)$$

Here $l = b/a$ represents the radius of the solid core to the radius of the semi-permeable sphere zone. When $l = 1$ the solid core occupies the entire spherical zone, and the semi-permeable zone vanishes. In other words, the region II vanishes. Essentially two cases are studied in this work. The first is the unbounded case: for which $r=l$, l is separation parameter ($=a/b$). The second is the bounded case (cell model) for which $r=l$, l is then termed a volume fraction.

4. EVALUATION OF DRAG FORCE

To determine the drag force resulting from the external flow acting on the surface of the inner solid core experienced by the couple stress fluid saturated porous medium, which will be oriented along the symmetrical axis, we define following Happel and Brenner [48], the integral:

$$F = 2\pi a^2 \int_0^\pi \left(\tau_{rr}^{(1)} \cos\theta - \tau_{r\theta}^{(1)} \sin\theta \right)_{r=a} \sin\theta d\theta. \quad (29)$$

Evaluation of the integral, leads to:

$$F_z = \frac{12\pi\mu U a \alpha^2 (l^3+2)(\lambda^2+\lambda(2+\tau)+2+\tau)}{2\left((2\alpha^2+1)\lambda^2+(2\alpha^2+1)\lambda(2+\tau)+l^3((\alpha^2-1)\lambda^2+(\alpha^2-1)\lambda(2+\tau)-2-\tau)+2+\tau\right)}. \quad (30)$$

Eqn. (30) is the drag force experienced on the semipermeable sphere (“particle”) engulfed by a couple stress fluid and generalizes the early result of [48] which only considered Newtonian fluids. Eqn. (30) can be normalized to give a dimensionless drag coefficient which is written as:

$$D_N = \frac{F_z}{-2\pi\mu U a}. \quad (31)$$

In full form we have:

$$D_N = \frac{6\alpha^2(l^3+2)(\lambda^2+\lambda(2+\tau)+2+\tau)}{2\left((2\alpha^2+1)\lambda^2+(2\alpha^2+1)\lambda(2+\tau)+l^3((\alpha^2-1)\lambda^2+(\alpha^2-1)\lambda(2+\tau)-2-\tau)+2+\tau\right)}. \quad (32)$$

5. EVALUATION OF VOLUMETRIC FLOW RATE

The volumetric flow rate through the semipermeable region is given by:

$$Q = u \cdot n ds = -2\pi U a^2 \psi^{(1)}(1,0). \quad (33)$$

Non-dimensional flow rate can be computed as follows:

$$Q_N = \frac{Q}{-\pi U a^2} = 1 + A_1 + A_2 + A_3 \left(1 + \frac{1}{\lambda}\right) e^{-\lambda}. \quad (34)$$

6. RESULTS AND DISCUSSION

Numerical evaluations using **Mathematica** software have been conducted. The results are visualized graphically in **Figs. 2-11** for the non-dimensional drag coefficient (D_N) and dimensionless flow rate (Q_N) behaviour. The effects of permeability (k), separation parameter (l), couple stress viscosity coefficient (η), couple stress inverse length dependent parameter ($\lambda = \sqrt{\mu/\eta}$) and couple stress viscosity ratio ($\tau = \eta/\eta'$) on these variables is addressed in sections 6.1 and 6.2. In section 6.3 streamline contours are computed in **Figs. 12-14** for various values of these parameters in addition to the inverse permeability parameter ($\alpha = 1/k$).

6.1 Effect of key parameters on non-dimensional drag coefficient (D_N):

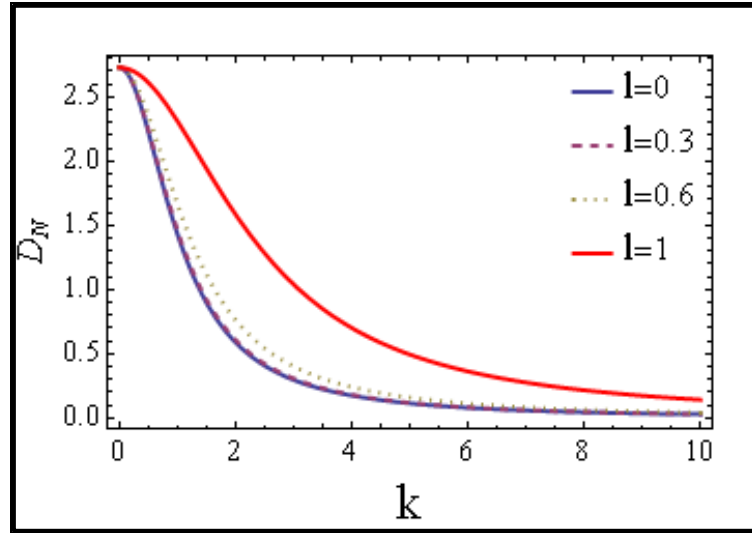


Fig. 2: The impact of permeability (k) and separation parameter (l) on non-dimensional drag (D_N).

Figure 2 shows the effect of the separation parameter on the non-dimensional drag within the enclosure containing a solid core for $\lambda = 3$ and $\tau = 0.5$. A significant influence is exerted on D_N with a change in separation parameter. Physically, for $l = 0$ (inner solid core radius $b \rightarrow 0$ i. e. the solid core vanishes) and the sphere changes into a hollow sphere. As l attains a value of 1, $b/a \rightarrow 1$ implying that the inner solid core now occupies the whole encased region replacing region II which vanishes). There is a significant elevation in drag D_N therefore as l increases from 0 to 1. The profiles are also strongly influenced with permeability (k). For small values of k i. e. tightly packed porous media with low permeability, the drag coefficient is maximum.

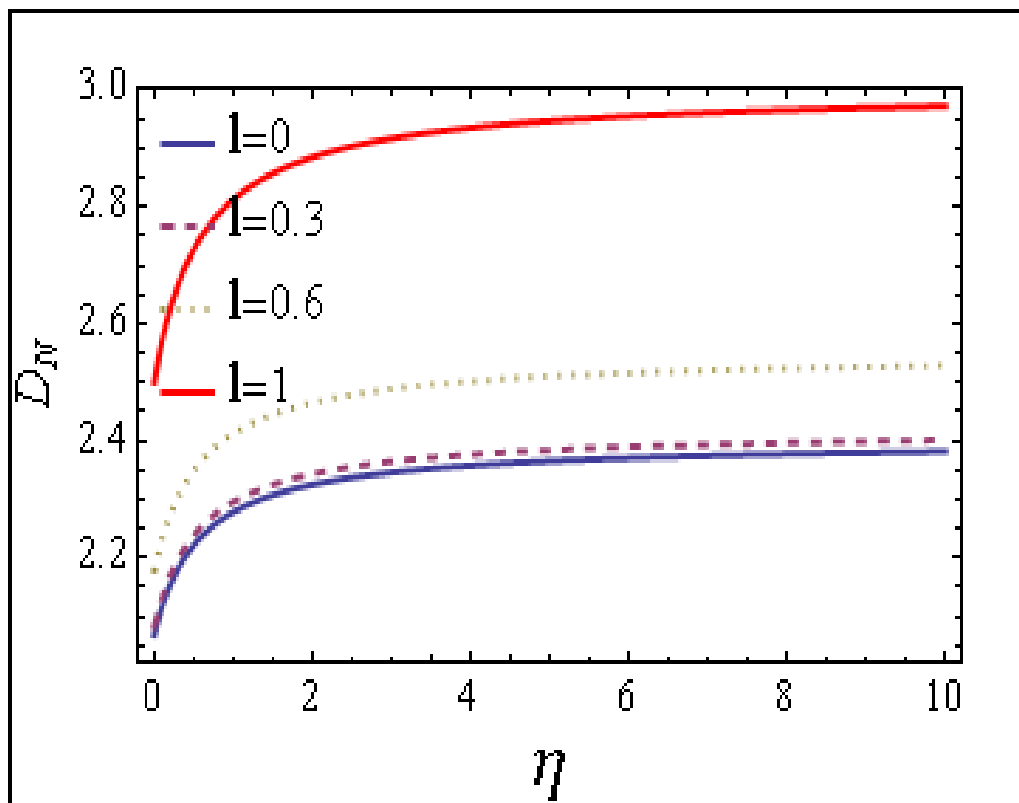


Fig. 3: The impact of couple stress viscosity (η) and separation parameter (l) on non-dimensional drag (D_N).

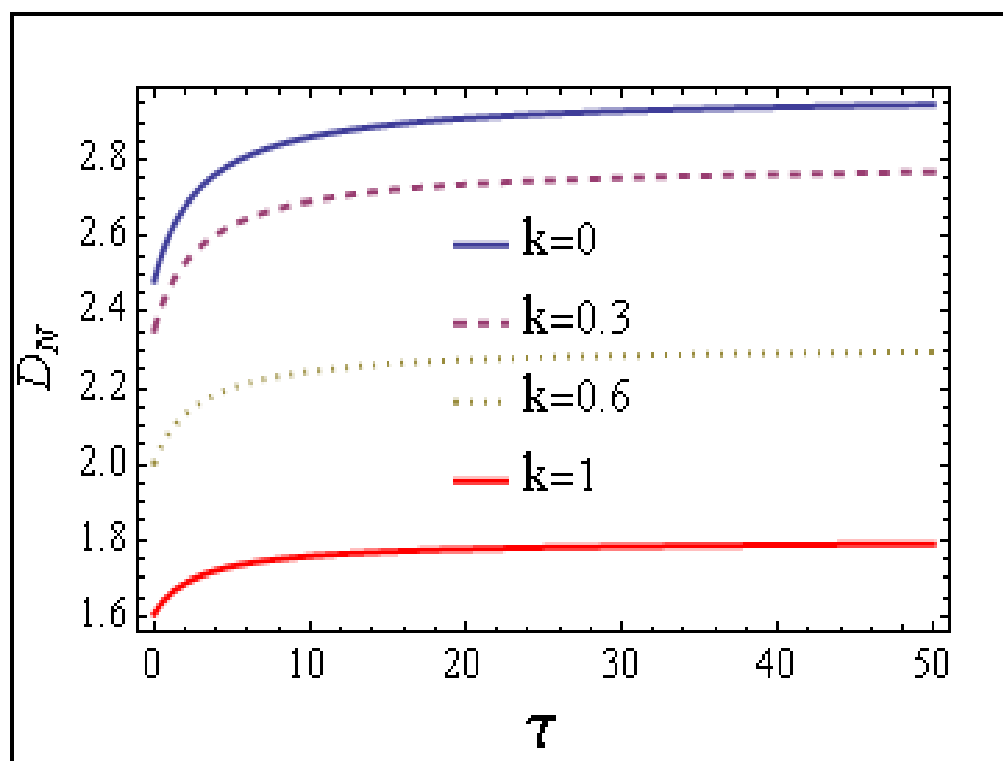


Fig. 4: The impact of couple stress viscosity ratio (τ) and permeability (k) on non-dimensional drag (D_N).

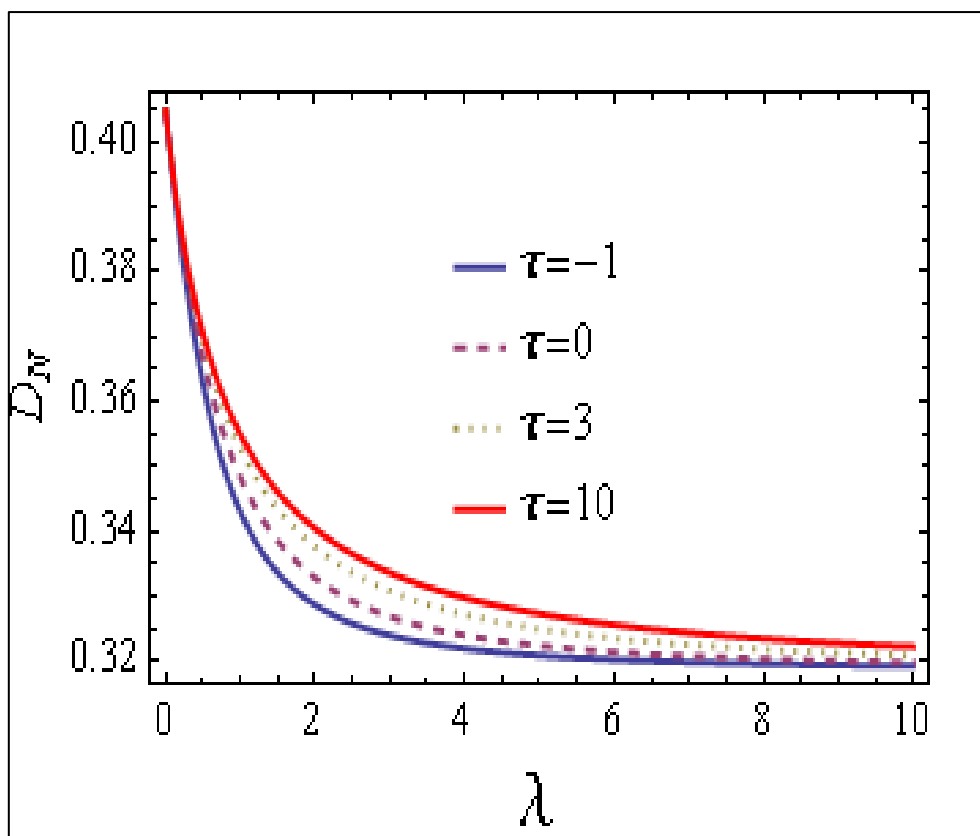


Fig. 5: The impact of couple stress viscosity ratio (τ) and couple stress viscosity parameter (λ) on non-dimensional drag (D_N).

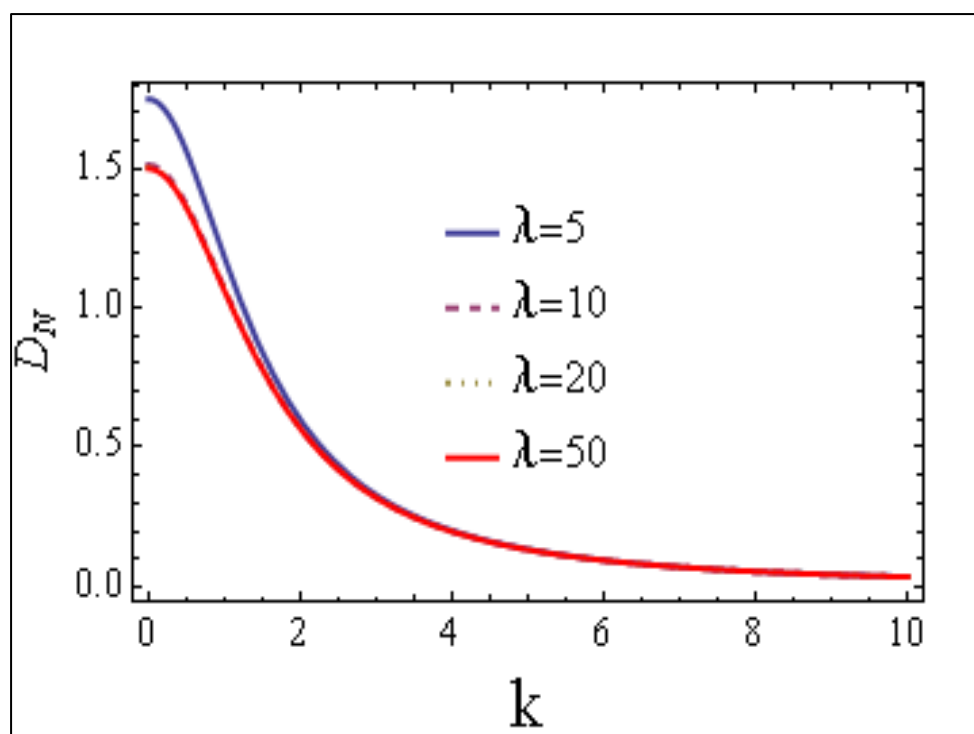


Fig. 6: The impact of couple stress viscosity parameter (λ) and permeability (k) on non-dimensional drag (D_N).

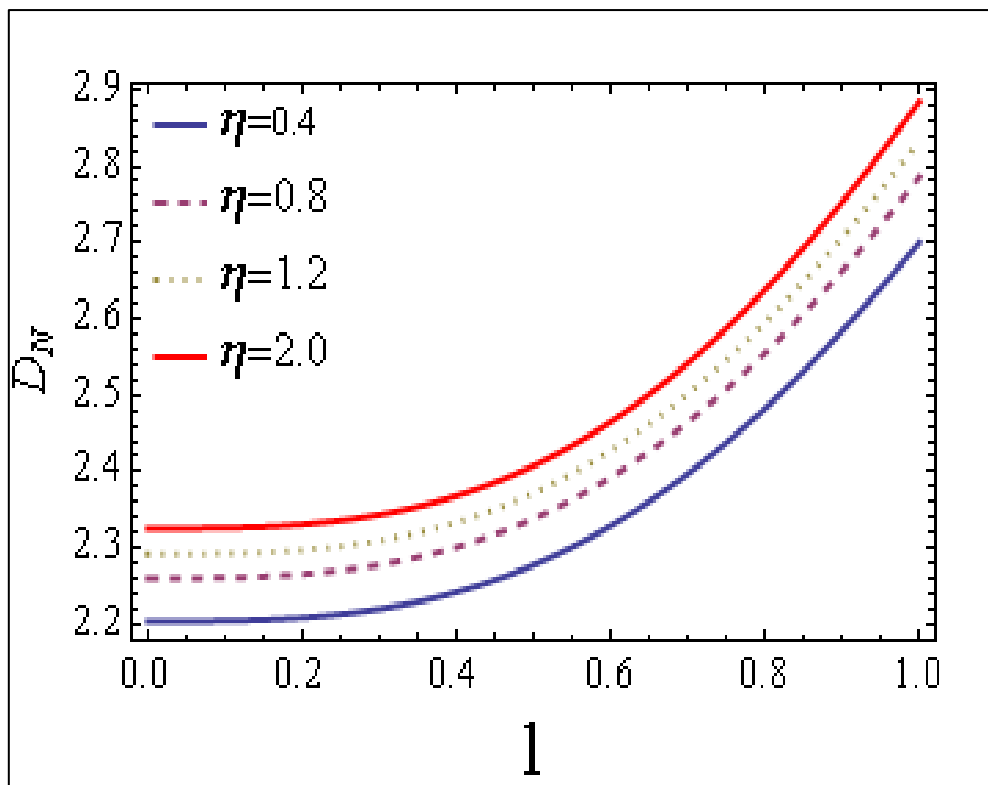


Fig. 7: The impact of couple stress viscosity (η) and separation parameter (l) on non-dimensional drag (D_N).

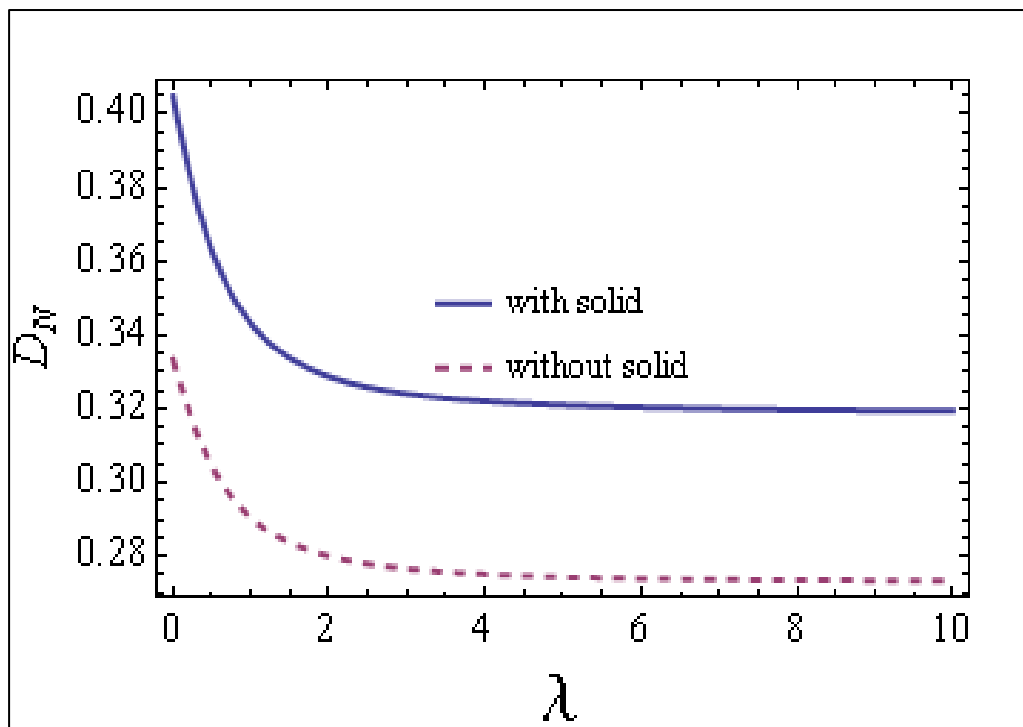


Fig. 8: Comparison of the drag for cases with a solid core and without solid core and for couple stress viscosity ratio parameter (λ)

As permeability, k increases, all profiles exhibit an asymptotic decay and there is a therefore a significant reduction in drag coefficient. Eventually a steady state is achieved at very high k values. There is clearly increasing impedance to the flow produced with lower permeability which is attributable to the presence of more fibres in the porous medium. These decelerate the percolating couple stress fluid. With higher permeability the porous medium is more sparsely packed, and this leads to a depletion in fibre resistance to the fluid and therefore lower D_N values. **Figure 3** represents the variation of non-dimensional drag D_N with couple stress viscosity (η) and different values of separation parameter ranging from $l = 0$, $l = 0.3$, $l = 0.6$ to the maximum of $l = 1$. Evidently the drag increases markedly with increment in couple stress viscosity implying that greater resistance is produced. A monotonic growth is observed at low values of (η) which morphs into a much gentler growth at higher values. The supplementary term, $-\eta \nabla^4 \vec{u}^{(1)}$, in the original momentum eqn. (1) indicates that couple stress viscosity opposes the flow. Couple stresses contribute to deceleration which results in a hike in drag coefficient. This has been confirmed in many other studies including Stokes [46, 47].

Couple stress fluid region with increasing the value of the viscosity parameter increases. As observed in Fig. 2, an increment in separation parameter (l) again produces a strong elevation in drag implying that much greater drag is produced for a fully solid core ($l = 1$, where external couple stress fluid is in direct contact only with the solid core) compared with the case where the solid core is absent ($l = 0$) and there is an interface only between the semi-permeable region II and the engulfing couple stress fluid. The presence of both an inner solid core and outer semi-permeable region (region II) corresponds to intermediate values of l (0.3, 0.6) and drag coefficient is between the other two limits on the plot. **Figure 4** confirms that the drag coefficient decreases with elevation in porous medium permeability (k) in the semi-permeable region II. The presence of more sparsely packed permeable material in region II can therefore be utilized to manipulate drag force and assist the flow. The couple stress viscosity ratio (τ) is also found to increase drag coefficient significantly implying again that couple stress viscosities are inhibitive to the flow i. e. they create extra resistance. Again, a steady state trend is attained at very high values of couple stress viscosity ratio implying that there is a limit to the opposing nature of the couple stresses in the regime. The collective influence of couple stress viscosity ratio (τ) and couple stress viscosity parameter (λ) on non-dimensional drag (D_N) is displayed in **Figure 5**. This figure clearly shows that the drag reaches its peak for $\lambda = 0$, whereas it is minimized at the maximum value of λ . This parameter is an inverse length dependent parameter ($\lambda = \sqrt{\mu/\eta}$). In other words when λ is high the length dependent effect of

couple stress fluids will be minimized and vice versa for when λ is low. This will contribute to the effects observed in Fig. 5 implying that as the flow tends to Newtonian (vanishing length dependence and high λ) the drag will be minimized. Again, the drag enhancement induced with couple stresses is therefore confirmed. **Figure 6** displays overall the resistance of the flow versus permeability (k) for different values of couple stress viscosity parameter (λ). The decreasing of the couple stress parameter plays a vital role in the non-dimensional drag which is strongly increased but only at very low permeability values (k). As permeability, k is increased the effect of λ is rapidly negated and all profiles merge. Therefore, at higher permeability values, the impact of couple stress viscosity is dominated by the permeability of the porous medium and couple stresses do not alter the drag coefficient tangibly. As the couple stress parameter λ increases it tends to a maximum (i.e., infinity) and in this limit the fluid becomes a viscous Newtonian fluid. **Figure 7** illustrates the variation of non-dimensional drag with both separation parameter (l) and couple stress viscosity (η). This figure clearly elucidates that there is a much lower drag coefficient for separation parameter $l < 0.5$. However very sharp escalation in the drag coefficient is incurred with separation parameter $l \geq 0.5$. The sensitivity of the drag force produced to the geometric configuration (solid core and surrounding semi-permeable sphere, which is controlled by the parameter $l = b/a$) is clearly captured. Physically it implies that as inner (solid core) sphere gets bigger the drag acting on the sphere increases. When $l = 1$, the composite sphere geometrically become a solid sphere and in the case the drag is a maximum.

Figure 8 provides a comparison of non-dimensional drag (D_N) both with and without a solid core versus couple stress viscosity ratio parameter (λ). It is abundantly clear that the drag is greater in the case of solid core than for the case of without solid core.

6.2 Effect of key parameters on non-dimensional flow rate (Q_N):

The effects of selected parameters on non-dimensional flow rate (Q_N) are shown in **figs. 9-11**. **Figure 9** displays the variation in volumetric flow rate (Q_N) with separation parameter (l) and couple stress fluid parameter (λ). It is apparent that flow rate decreases as radius of the inner solid core sphere (b) increases i. e. as l values increase. This is the reverse trend to the influence on the drag coefficient (which is increased) as computed earlier. The volumetric flux of fluid is clearly reduced as the inner solid core occupies an increasing of region II and then in the limit, $l = 1$ actually replaces the outer semi-permeable region II (the composite sphere geometrically becomes a solid sphere). For this case, volumetric flow rate must therefore

become a minimum. With increasing couple stress parameter (λ) there is a sharp depletion in volumetric flow rate values, but this strong downtrend is maximized at much higher values of separation parameter (l). At lower values of l , the profiles while they are reduced are not modified as significantly with an increase in couple stress parameter (λ) and exhibit a plateau-like topology.

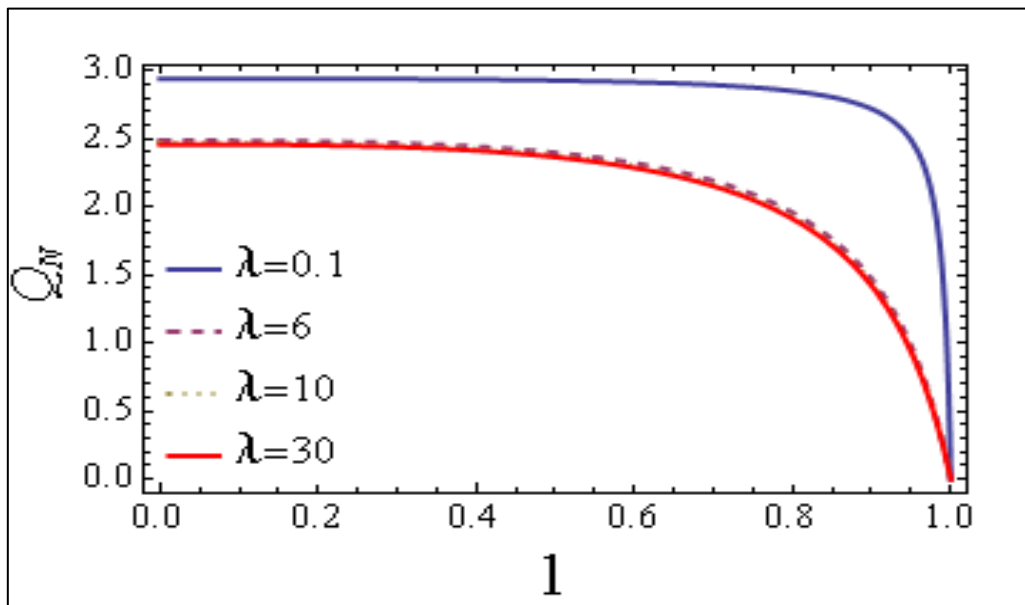


Fig. 9: Influence of couple stress viscosity ratio parameter (λ) and separation parameter (l) on non-dimensional flow rate (Q_N)

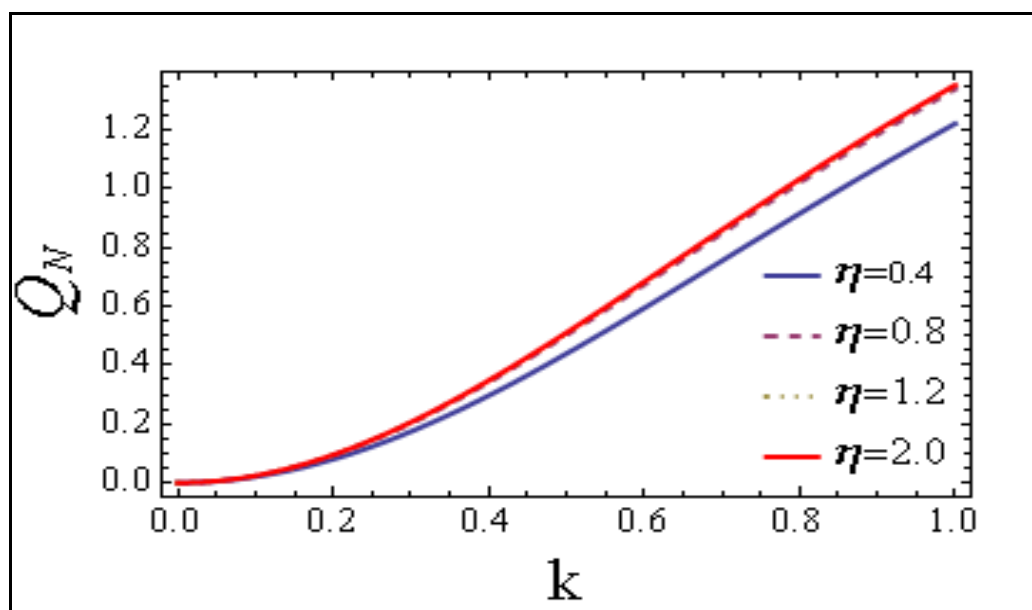


Fig. 10: Influence of couple stress viscosity (η) and permeability parameter (k) on non-dimensional flow rate (Q_N)

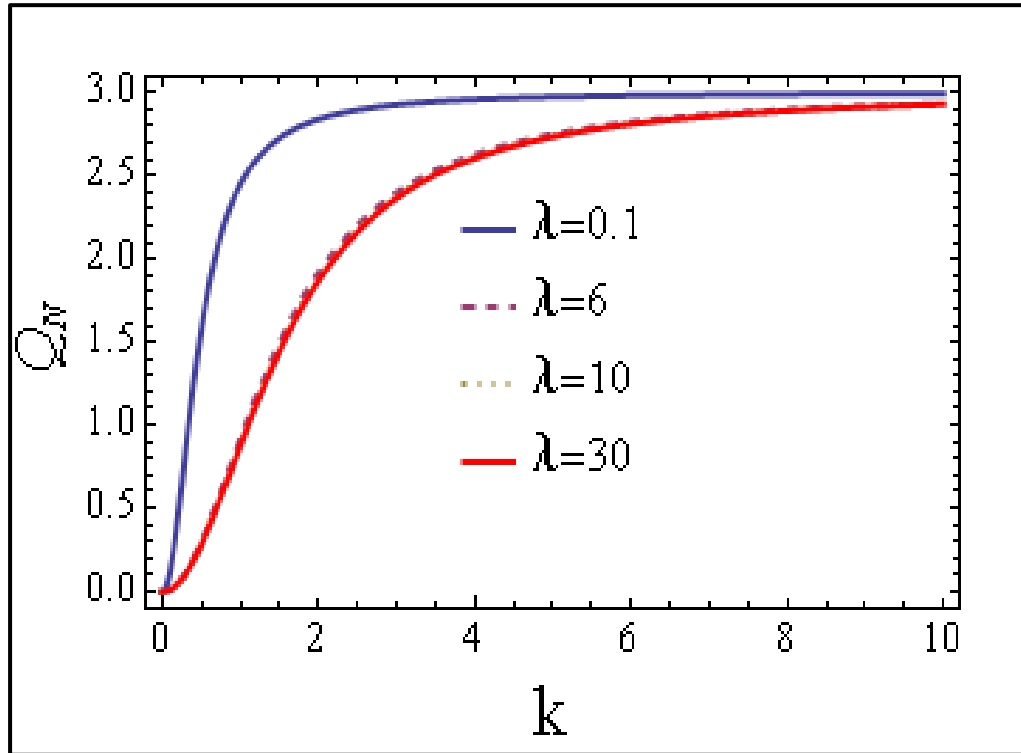


Fig. 11: Influence of couple stress viscosity ratio parameter (λ) and permeability (k) on non-dimensional flow rate (Q_N)

Figure 10 shows the effect of the permeability (k) on the flow rate with the various values of couple stress viscosity (η) ranging from 0.4, 0.8, 1.2 to 2.0. It is noted that the flow rate is strongly enhanced as the permeability of the sphere region II increases. Higher permeability clearly encourages the percolation of couple stress fluid since less fiber impedance is present. It is also noteworthy that an increment in flow rate is also achieved with higher values of couple stress viscosity, although the effect is clearly amplified at higher permeability (k). Flow rate is therefore minimized for low couple stress viscosity ($\eta = 0.4$) and very low permeabilities ($k < 0.3$). The greatest enhancement is computed in the range between $\eta = 0.8$ to $\eta = 2$ indicating that stronger couple stresses boost the flux of the fluid.

Figure 11 depicts graphically the variation of the flow rate Q_N against the permeability k for diverse values of couple stress parameter (λ) with $l = 0.5$ (i. e. the solid sphere is exactly half the radius of the outer semipermeable region II). Evidently the flow rate increases as permeability k increases. However, the rate of flow decreases as couple stress parameter λ increases although the effect diminishes with greater permeability. The depression induced in flow rate with increment in couple stress parameter (λ) is maximum when the permeability is very low for the region II. We noted that the flow rate is a minimum in the case of an

impermeable outer sphere ($k \rightarrow 0$). The opposite case of infinite permeability i. e. purely fluid region II corresponds to $k \rightarrow \infty$ but is not computed since the trend established with high finite values of k up to 10 is sufficient to establish the nature of the hydrodynamics at very high permeabilities. Overall, the flow rate is greater in the case of a permeable sphere (region II).

6.3 Effects of selected parameters on streamline contour patterns

The streamline patterns are displayed in **Figures 12-14** for various parameters.

Fig. 12 depicts the influence of separation parameter (l) on streamline contours with fixed values of $\alpha = 0.1$, $\lambda = 2$, and $\eta = 5$. The hydrodynamic flow patterns are uniformly affected initially with a small increment in separation parameter [$l = 0.05$ and $l = 0.1$] and there is a slight clustering of streamlines computed towards the solid core. However, with further increment in separation parameter l to higher values of 0.5 , 0.8 and $l = 1$ the flow patterns are increasingly disturbed, and an increasingly strong dual vortex structure is synthesized with a symmetrical pattern on either side.

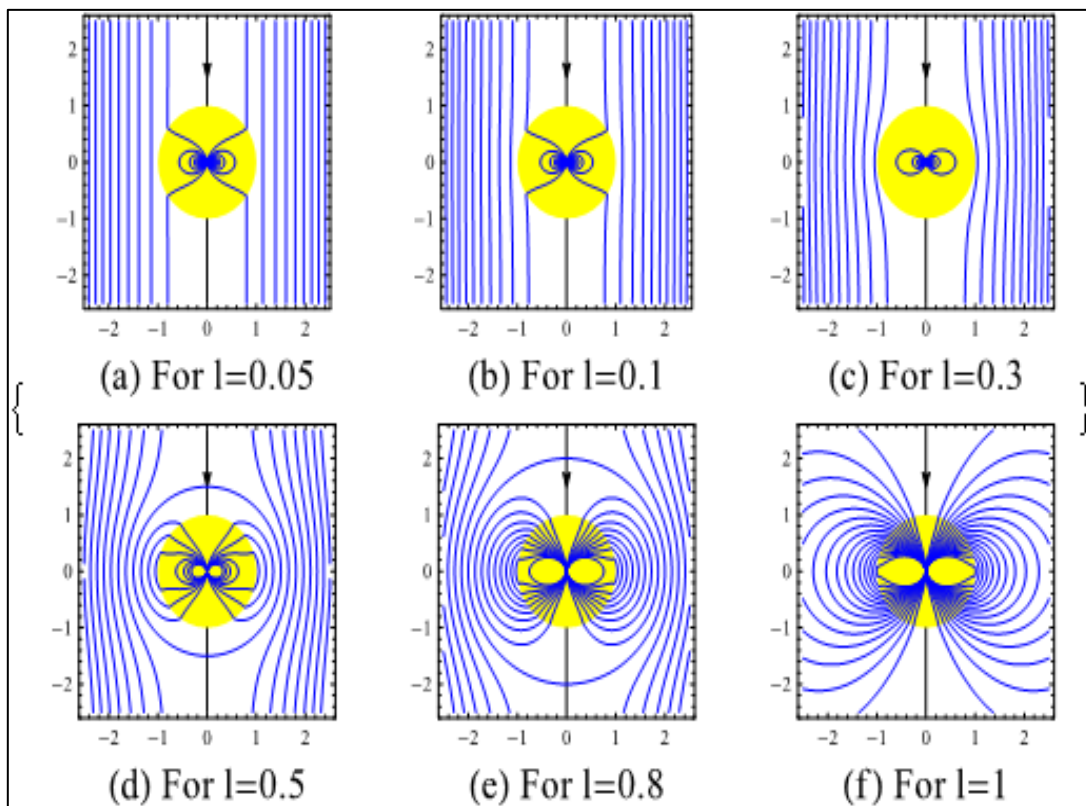


Fig. 12: Streamlines for various separation parameter (l)

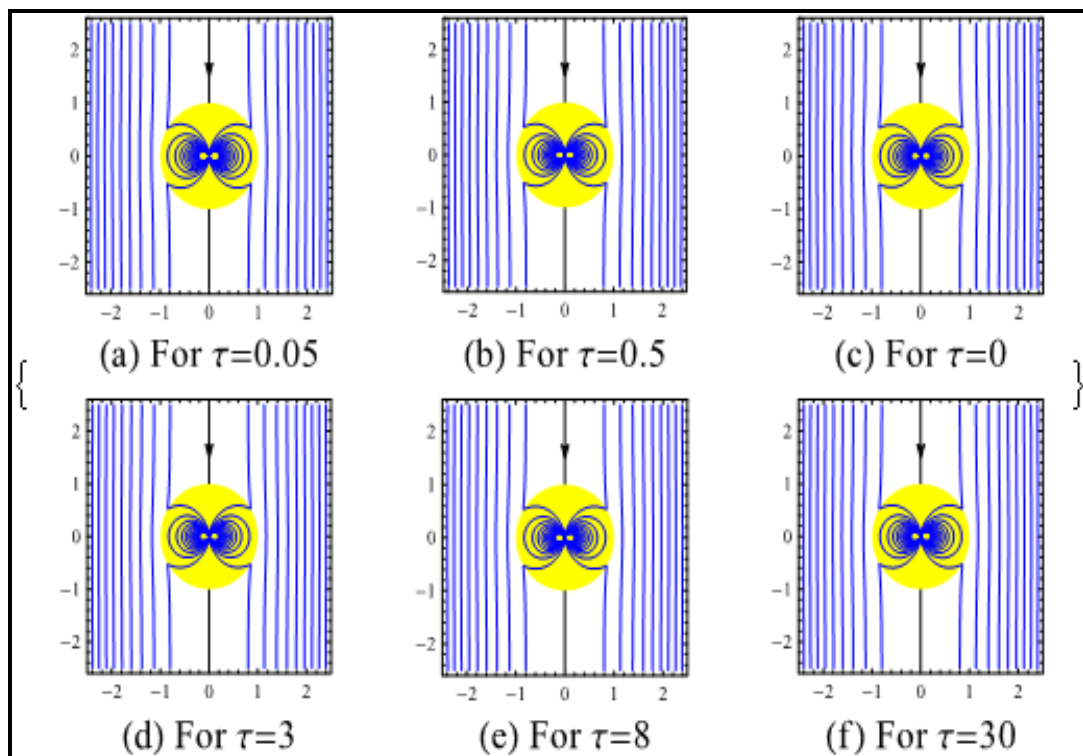


Fig. 13: Streamlines for various couple stress viscosity ratio (τ)

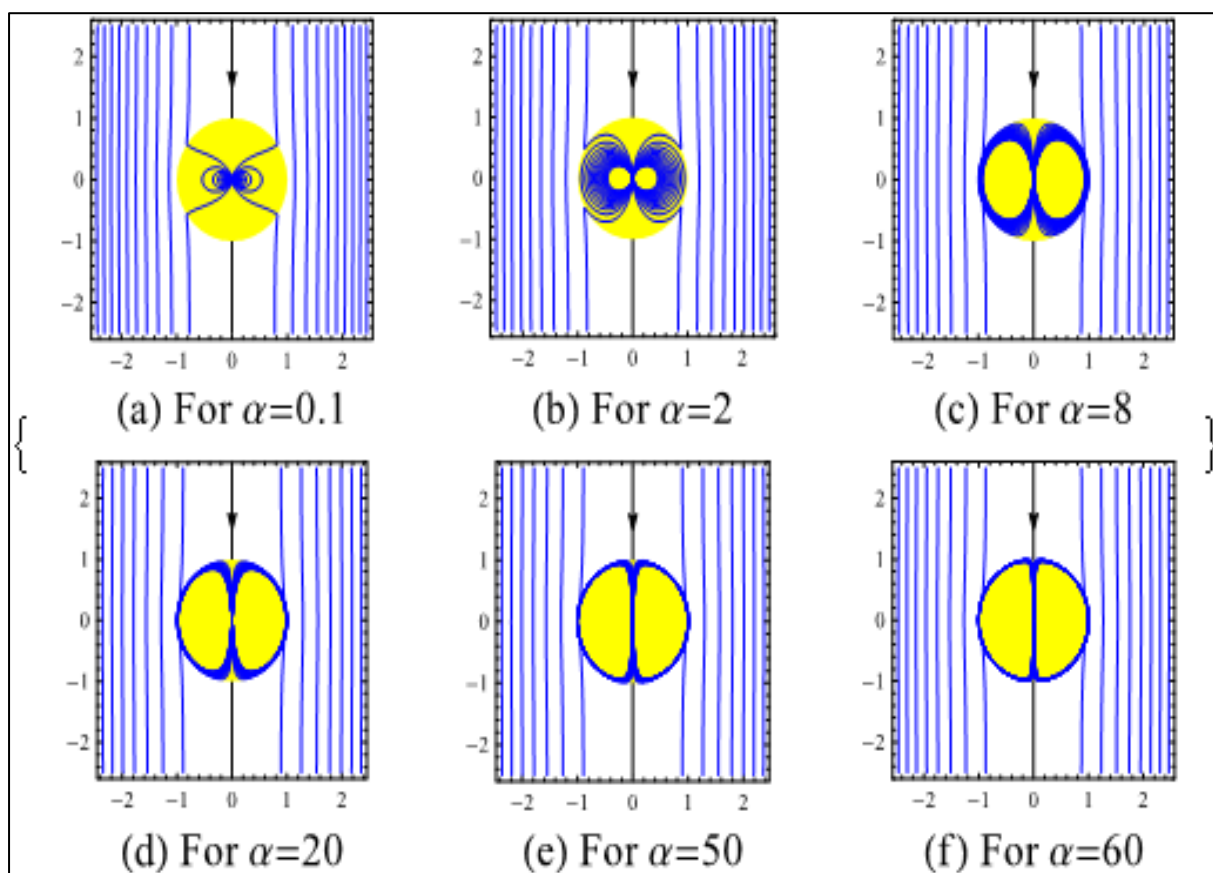


Fig. 14: Streamlines for various inverse permeability parameter ($\alpha = 1/k$)

Figure 13 illustrates the effect of couple stress viscosity ratio $\tau = (\frac{\eta}{\eta'})$ on the streamline with fixed values of $\lambda = 2$, $\alpha = 0.1$. When couple stress viscosity ratio $\tau = 0.05$ the flow of the streamlines is perturbed in the semipermeable region II. With a large increment in couple stress viscosity parameter, the streamlines are not markedly modified i. e. the streamline patterns remain almost uniform with minimal distortion with increasing couple stress viscosity ratio.

Figure 14 visualizes the effect of inverse permeability parameter (α) on streamline contours. Increasingly the initial distortion in flow patterns around the sphere are strongly damped out. Initially for semi permeable parameter $\alpha = 0.1$ the couple stress fluid penetrates weakly in the semi permeable medium (region II). However, for larger values of α (0.1, 2, 8, 20, 50, and 60) the couple stress fluid completed penetrates more strongly into the semipermeable medium and it becomes increasingly closer to the solid inner sphere. This stabilizes the flow patterns.

7. CONCLUSIONS

Motivated by applications in non-Newtonian chemical engineering processes involving emulsion droplet motion in porous media, a mathematical model has been developed for steady-axisymmetric creeping Stokesian flow of a couple stress fluid external to a semi-permeable sphere saturated with couple stress fluid and containing a solid core. The Darcy-Brinkman formulation is adopted for the porous medium. Analytical expressions are derived for dimensionless pressure, tangential stress and the couple stress components using the method of separation of variables and Gegenbauer functions of the first kind. The integration constants are evaluated with appropriate boundary conditions on the inner and outer boundary of the semi-permeable zone with the aid of Mathematica symbolic software. Solutions for the drag force exerted by the couple stress fluid on the semi-permeable sphere and volumetric flow rate are also derived with corresponding expressions for the drag coefficient and non-dimensional volumetric flow rate. Extensive visualization is included additionally for streamline contours. The present work generalizes the earlier study of Krishnan and Shukla [21] to consider porous medium permeability effects, with the inclusion of a permeable outer sphere. The present analysis has shown that:

1. As the separation parameter (l) increases, the non-dimensional drag within the semi permeable layer is increased.
2. An increase in couple stress fluid parameter reduces the non-dimensional drag within the solid core.

3. The drag experienced with a solid core present is greater than when it is absent.
4. Drag coefficient is observed to decrease with increment in permeability (k) owing to the reduced resistance of porous medium fibers to the flow
5. With increase in couple stress viscosity parameter (η) and couple stress viscosity ratio (τ) the drag coefficient is sharply increased initially but attains an asymptotic limit at very high values of these parameters.
6. With the increase in couple stress fluid viscosity (η) and permeability parameter (k), the flow rate increases.
7. The reduction induced in flow rate with increment in couple stress parameter (λ) is maximum when the permeability is very low.
8. Streamline patterns are most strongly influenced by the separation parameter (l) and only weakly modified with permeability parameter (α) and couple stress viscosity ratio (τ).
9. The permeability of region II (outer sphere) can be manipulated to considerably modify drag and volumetric flow characteristics in practical chemical engineering systems.

The present work has revealed some interesting features of Stokesian dynamics of couple stress fluids with permeability and solid core effects. However, porosity of the porous medium has been ignored. Furthermore, there are a diverse range of alternative rheological models relevant to characterizing the non-Newtonian behaviour which include Bingham viscoplastic models [49] and FENE-P viscoelastic models [50]. Furthermore, magnetohydrodynamic effects may also be considered in future studies, following the excellent recent work of Maurya *et al.* [51]. Additionally, wall slip effects and non-Newtonian nanofluids such as Maxwell viscoelastic, Reiner-Rivlin second grade and Williamson shear-thinning nano-liquids ([52]-[54]) which are growing in interest in chemical engineering may also be considered. These areas are currently being explored and efforts in these directions will be communicated imminently.

ACKNOWLEDGEMENTS

The authors appreciate the comments of the reviewers which have improved the clarity of the present work. The second author (OAB) also wishes to acknowledge the support of his sister, Tasveer Bég and colleagues Dr. Sireetorn Kuharat and Dr. Ali Kadir, during the original preparation of the article, for many excellent discussions regarding creeping hydrodynamics. The second author also wishes to express his gratitude to the late Professor Howard Brenner of MIT who originally got him interested in creeping non-Newtonian hydrodynamics during many meetings in 2001.

REFERENCES

- [1] Stokes VK, Couple stresses in fluids, *Phys Fluids*, 9:1709-1715 (1966).
- [2] A.C. Eringen, *Microcontinuum Field Theories-II Fluent Media*, Springer, New York (2001).
- [3] A.C. Eringen, Theory of micropolar fluids, *J. Math. Mech*, 16, 1-8 (1966).
- [4] Naduvinamani NB, Patil SB, Numerical solution of finite modified Reynolds equation for couple stress squeeze film lubrication of porous journal bearings, *Computers and Structures*, 87:1287-1295 (2009).
- [5] Walicki, E and Walicka, A., Inertial effect in the squeeze film of couple stress fluids in biological bearings. *Int. J. Appl. Mech. Engg.* 4, 363-373 (1999).
- [6] J.-R. Lin and C.-R. Hung, Combined effects of non-Newtonian couple stresses and fluid inertia on the squeeze film characteristics between a long cylinder and an infinite plate, *Fluid Dynamics Research*, vol. 39, no. 8, pp. 616–639 (2007).
- [7] O. Anwar Bég, S.K. Ghosh, S. Ahmed and T. A. Bég, Mathematical modelling of oscillatory magneto-convection of a couple stress biofluid in an inclined rotating channel, *J. Mechanics In Medicine and Biology*, 12 (3), 1250050-1 to 1250050-35 (2012).
- [8] N. Ali, M. Sajid, Z. Abbas and O. Anwar Bég, Swimming of micro-organism in a fluid with couple stresses - a rheological model of embryological hydrodynamic propulsion, *J. Mechanics in Medicine and Biology*, 17 (3) 1750054 (2017).
- [9] J. V. Ramana Murthy, J. Srinivas and O. Anwar Bég, Entropy generation analysis of radiative heat transfer effects on channel flow of two immiscible couple stress fluids, *J. Brazilian Soc. Mech Sci. Eng*, 39, 2191–2202 (2017).
- [10] Nagaraju G and Matta A and Kaladhar K., Effects of chemical reaction and thermal radiation on heat generated stretching sheet in a couple stress fluid flows. *Frontiers in Heat and Mass Transfer*; 7: 1-5 (2016).
- [11] D. Tripathi, R. Jhorar, O. Anwar Bég and A. Kadir, Electro-magneto-hydrodynamic peristaltic pumping of couple stress biofluids through a complex wavy micro-channel, *J. Molecular Liquids*, 236, 358-367 (2017).
- [12] L. Iyenger, Analytical and computational studies in couple stress fluid flows. *U.G.C Research Project C-8-4/82 SR III*, (1985)
- [13] Iyengar T K V and Srinivasa Charya D (1993) Stokes flow of an incompressible micropolar fluid past an approximate sphere. *International Journal of Engineering Science*; 31(1): 115-123.
- [14] Ramkissoon H (1978) Drag in couple stress fluids. *ZAMP- Journal of Applied Mathematics and Physics*; 29: 341-346.

- [15] Devakar M and Iyengar T K V (2008) Stokes problems for an incompressible couple stress fluid. *Nonlinear Analysis: Modelling and Control*; 1: 181-190.
- [16] Devakar M and Iyengar T K V (2010) Run up flow of a couple stress fluid between parallel plates. *Non-Linear Anal.: Model Control*; 15: 29-37.
- [17] Iyengar T K V and Geetha Vani V (2012) Flow of an incompressible couple stress fluid in the region between two slowly rotating confocal oblate spheroids. *Global Journal of Mathematical Sciences: Theory and Practical*; 4: 337-352.
- [18] Devakar M, Sreenivasu D and Shankar B (2014) Analytical solutions of couple stress fluid flows with slip boundary conditions. *Alexandria Engineering Journal*; 53: 723- 730.
- [19] Ashmawy E A (2016) Drag on a slip spherical particle moving in a couple stress fluid. *Alexandria Engineering Journal*; 55: 1159-1164.
- [20] Geetha Vani V and Ravi Kant A S V (2020) Oscillatory flow of an incompressible couple stress fluid generated by the rotary oscillations of two concentric spheres. *AIP Conference Proceedings*; 2277, 030020.
- [21] Ramalakshmi K and Shukla P (2021) Creeping flow of couple stress fluid past a fluid sphere with a solid core: *ZAMM*; 101: e202000115.
- [22] Darcy H (1856) *Les Fontaines Publiques De La Ville De Dijon*. Paris, Victor Dalmont.
- [23] Brinkman H C (1947) A calculation of viscous force exerted by a flowing fluid on dense swarm of particles. *Appl. Sci. Res*; A1: 27-34.
- [24] W. Carman, Fluid flow through granular beds, *Trans. Amer. Inst. Chem. Engrs.* **15**, 150, (1937).
- [26] Joseph D and Tao L (1964) The effect of permeability on the slow motion of a porous sphere in a viscous liquid: *ZAMM- Z. Appl. Math. Mech*; 44: 361-364.
- [26] Tam C (1969) The drag on a cloud of spherical particles in a low Reynolds number flow. *Journal of Fluid Mechanics*; 38: 537-546.
- [27] Lundgren T (1972) Slow flow through stationary random beds and suspensions of spheres, *Journal of Fluid Mechanics*; 51, 273-299.
- [28] A. Raptis and H.S. Takhar, Polar fluid through a porous medium, *Acta Mechanica*, 135, 91–93 (1999).
- [29] Hiremath PS, Patil PM, Free convection effects on the oscillatory flow of a couple stress fluid through a porous medium, *Acta Mechanica* 98:143-158 (1993).
- [30] J.C. Umavathi and O. Anwar Bég, Simulation of the onset of convection in porous medium layer saturated by a couple stress nanofluid, *Microfluidics and Nanofluidics* (2021). 25:53 <https://doi.org/10.1007/s10404-021-02448-5> (20 pages).

- [31] Srinivasacharya D and Rajyalakshmi I (2004) Creeping flow of micropolar fluid past a porous sphere, *Applied Mathematics and Computation*; 153: 843-854.
- [32] Gupta B R and Deo S (2010) Stokes flow of micropolar fluid past a porous sphere with non-zero boundary condition for microrotations. *International Journal of Fluid Mechanics Research*; 37: 424-434.
- [33] Aparna P, Ramana Murthy J V and Sreelatha K (2007) Uniform flow of an incompressible couple stress fluid past a permeable sphere. *International Electronic Engineering Mathematical Society*; 8: 1-10.
- [34] Aparna P and Ramana Murthy J V G (2008) Oscillatory flow of an incompressible couple stress fluid past a permeable sphere. *Proceedings of 53rd Congress ISTAM, Osmania University, India*; 6: 164-173.
- [35] Radhika T S V and Iyengar T K V (2010) Stokes flow of an incompressible couple stress fluid past a porous spheroidal shell. In: *Proceedings of international multi-conference of engineers and computer scientists, IMECS, Hong Kong*; 3: 17-19.
- [36] Selvi, R and Shukla P (2017) Drag on a fluid sphere embedded in porous medium with zero spin condition. *International Journal of Pure and Applied Mathematics*; 109: 171-179.
- [37] Selvi R and Shukla P and Singh A K (2020) Drag on a Reiner-Rivlin liquid sphere embedded in a porous region placed in a micropolar fluid. *J. Porous Media*; 23: 613-626.
- [38] Selvi R and Shukla P and Fillipov A N (2020) Flow around a liquid sphere filled with a non-Newtonian liquid and placed into a porous medium. *Colloid Jour*; 82: 152-160.
- [39] Selvi R and Shukla P (2022) Analytical Solutions of Non-Newtonian Fluid through a Reiner-Rivlin Liquid Sphere with Cell Surface. *IAENG International Journal of Applied Mathematics*; 52: 811-816.
- [40] Shreen El-Sapa and Noura Alsudais S (2021) Effect of magnetic field on the motion of two rigid spheres embedded in porous media with slip surfaces. *The European Physical Journal. E, Soft matter*; 44: 1-11.
- [41] Namdeo R P and Gupta B R (2021) Creeping flow around a spherical particle covered by semipermeable shell in presence of magnetic field. *IOP Conf. Series: Materials Science and Engineering*; 1136: 012032.
- [42] Krishna Prasad Madasu and Priya Sarkar (2022) Couple stress fluid past a sphere embedded in a porous medium. *Archive of Mechanical Engineering*; 69: 5-19.
- [43] Sakthivel Shyamala and Shukla Pankaj (2022) Drag on a porous sphere embedded in couple stress fluid. *Journal of Porous Media*; 25: 105-115.
- [44] Z. Qi *et al.*, Lattice Boltzmann investigation of non-Newtonian fluid flow through a packed bed of uniform spheres, *Powder Technology*, 343, 225-236 (2019).

- [45] Setukha A, Tretiakova R. Computational modeling of lymph filtration and absorption in the lymph node by boundary integral equations. *Algorithms*. 2022; 15(10):388.
- [46] Stokes V K (1971) Effects of couple stresses in fluids on the creeping flow past a sphere. *Phys. Fluids*; 14: 1580-1582.
- [47] Stokes V K (1984) *Theories of Fluids with Microstructure*, Springer, New York (1984).
- [48] Happel J and Brenner H (1965) *Low Reynolds Number Hydrodynamics*. Englewood Cliffs, NJ: Prentice-Hall.
- [49] Roy A K, Debnath S. and Bég O. Anwar, (2023) Transient solute dispersion in electro-osmotic viscoplastic flow in a microchannel. *ZAMM. Journal of Applied Mathematics and Mechanics*. doi.org/10.1002/zamm.202200260.
- [50] M. Norouzi. S. Z. Daghighi. O. Anwar Bég Exact analysis of heat convection of viscoelastic FENE-P fluids through isothermal slits and tubes, *Meccanica*, 53, 817-831 (2018).
- [51] Maurya P.K.; Deo, S. and Maurya D.K. (2023): Couple stress fluid flow enclosing a solid sphere in a porous medium: Effect of magnetic field. *Physics of Fluids*, 35, 072006.
- [52] M. Waqas *et al.*, Chemically reactive Squeezed flow of Maxwell nanofluid confined by parallel stratified walls subjected to radiative flux, *Tribology International*, 189, (2023) 108986.
- [53] M. Waqas *et al.*, Darcy-Forchheimer magnetized flow based on differential type nanoliquid capturing Ohmic dissipation effects, *Propulsion and Power Research*, 12, (2023) 443-455.
- [54] W.A. Khan, Evaluating the characteristics of magnetic dipole for shear-thinning Williamson nanofluid with thermal radiation, *Computer Methods and Programs in Biomedicine*, 191, (2020) 105396.